Estuarine, Coastal and Shelf Science 197 (2017) 221–235

Contents lists available at ScienceDirect

Estuarine, Coastal and Shelf Science

journal homepage: www.elsevier.com/locate/ecss

Field estimates of floc dynamics and settling velocities in a tidal creek with significant along-channel gradients in velocity and SPM

C. Schwarz [a, c, *], T. Cox [a, b], T. van Engeland [a, b], D. van Oevelen [b], J. van Belzen [b], J. van de Koppel [b], K. Soetaert [b], T.J. Bouma [b], P. Meire [a], S. Temmerman [a]

[a] Ecosystem Management Research Group, University of Antwerp, Universiteitsplein 1, 2610 Wilrijk, Belgium
[b] NIOZ Royal Netherlands Institute for Sea Research, Department of Estuarine and Delta Systems, and Utrecht University, P.O. Box 140, 4400 AC Yerseke, The Netherlands
[c] Faculty of Geosciences, Universiteit Utrecht, 3508 TC Utrecht, The Netherlands

ARTICLE INFO

Article history:
Received 9 December 2016
Received in revised form
16 August 2017
Accepted 22 August 2017
Available online 24 August 2017

ABSTRACT

A short-term intensive measurement campaign focused on flow, turbulence, suspended particle concentration, floc dynamics and settling velocities were carried out in a brackish intertidal creek draining into the main channel of the Scheldt estuary. We compare *in situ* estimates of settling velocities between a laser diffraction (LISST) and an acoustic Doppler technique (ADV) at 20 and 40 cm above bottom (cmab). The temporal variation in settling velocity estimated were compared over one tidal cycle, with a maximum flood velocity of 0.46 m s^{-1}, a maximum horizontal ebb velocity of 0.35 m s^{-1} and a maximum water depth at high water slack of 2.41 m. Results suggest that flocculation processes play an important role in controlling sediment transport processes in the measured intertidal creek. During high-water slack, particles flocculated to sizes up to 190 μm, whereas at maximum flood and maximum ebb tidal stage floc sizes only reached up to 55 μm and 71 μm respectively. These large differences indicate that flocculation processes are mainly governed by turbulence-induced shear rate. In this study, we specifically recognize the importance of along-channel gradients that places constraints on the application of the acoustic Doppler technique due to conflicts with the underlying assumptions. Along-channel gradients were assessed by additional measurements at a second location and scaling arguments which could be used as an indication whether the Reynolds-flux method is applicable. We further show the potential impact of along-channel advection of flocs out of equilibrium with local hydrodynamics influencing overall floc sizes.

1. Introduction

Estuaries interface the terrestrial, riverine and marine environments. They consist of channels, tidal flats and tidal wetlands, and can act as temporary storage or sink for particles of riverine or marine origin (Stevenson et al., 1988; Woodruff et al., 2001). Fine sedimentary cohesive particles found in estuaries, exert a significant impact on bio-geochemical-, ecological, morphodynamic and eco-morphodynamic processes and are therefore of significant importance for coastal and estuarine management (e.g. harbors and navigation channels, coastal protection but see (Avoine et al., 1981; De Vriend et al., 2011; Einstein and Krone, 1962; Hibma et al., 2004; Nardin and Edmonds, 2014; Winterwerp and van Kesteren, 2004):). Cohesive sediment particles differ in their behavior from non-cohesive particles due to their ability to flocculate (Eisma, 1986; Fettweis and Baeye, 2015). Cohesive sediments consist of a mixture of clay, silt, fine sand, organic material and sometimes gas. Their clay minerals and organic matter are responsible for the cohesive behavior through electrostatic and Vanderwaals forces and sticky extracellular polymeric substances (Winterwerp and van Kesteren, 2004).

Flocculation in dynamic environments, such as estuaries, is mainly dependent on the balance between floc-aggregation and floc-destruction, which is governed by the relation between turbulence intensity and the concentration of suspended particles. For instance turbulent motions will cause particles, carried by eddies to collide and form flocs (Hill et al., 1992). On the other hand turbulent

* Corresponding author. Faculty of Geosciences, Universiteit Utrecht, 3508 TC Utrecht, The Netherlands.
E-mail address: c.s.schwarz@uu.nl (C. Schwarz).

http://dx.doi.org/10.1016/j.ecss.2017.08.041
0272-7714/

shear may also disrupt flocs, causing them to break up into smaller flocs or primary particles (Verney et al., 2011; Winterwerp, 2002). Moreover increasing suspended particle concentration at low turbulence levels promotes floc growth, but increasing turbulence together with increasing suspended particle concentrations causes floc disruption (Dyer and Manning, 1999). Flocculation contributes significantly to the settling flux in the sedimentation-resuspension cycle, by altering particle/aggregate settling velocities, transport and sedimentation-erosion behavior. Therefore, the size and porosity of flocculated aggregates and their associated settling velocities are crucial parameters in numerical models that simulate and predict sediment transport (e.g (Burchard et al., 2008; Van Rijn, 1993).). Moreover, these processes do not only govern short-term transport processes but are also major determinants of the long-term morphological evolution of the estuarine bio-geomorphology (Christiansen et al., 2000; Graham and Manning, 2007; Wang et al., 2013). An improved understanding of the physical processes governing sedimentation-resuspension processes and specifically flocculation and settling behavior in an estuarine setting is therefore needed (Wang et al., 2013).

A myriad of studies has been conducted to understand particle settling behavior, the influence of flocculation on them, and its importance for long-term morphological evolution. Historically, the focus in flocculation mediated settling of cohesive particles was on physical processes, such as suspended particulate matter concentration (further referred to as SPM) and turbulence (Dyer, 1995). Hereafter, settling velocity has been described as a function of SPM concentration, based on the theory that with increasing SPM concentration, more collisions between suspended primary particles can occur, hence facilitating flocculation and increasing settling velocities, until critically high SPM concentrations are reached for which so-called hindered settling and reduced settling velocities occur (e.g. Einstein and Krone, 1962; Eisma et al., 1997; Van Leussen, 1988). Turbulence, Brownian motion and differential settling have been shown to facilitate flocculation by increasing particle collision leading to floc aggregation (Winterwerp, 2002). However when critical turbulence levels are exceeded, flocs are destroyed (Eisma et al., 1991; Winterwerp, 2002, 1998). It was moreover shown that factors such as sediment composition (e.g. organic matter content), salinity or pH have significant implications for floc formation. For instance Eisma (1986) showed that large estuarine flocs mainly consist of flocculated micro-flocs with mineral grains as the most important constituent, however that maximum floc size is highly dependent on the amount of organic matter and the type of clay minerals present. This was also confirmed and extended by Mietta et al. (2009), who showed that mean floc size increases with increasing organic matter content and decreasing pH. The presence of organic matter also has important implications for the settling velocities, specifically it was shown that the mixture of organic matter and mineral particles settles faster than either of this constituents alone (Eisma, 1986). Field studies have documented the importance of both SPM controlled (e.g (Dyer and Manning, 1999).), as well as turbulence controlled flocculation (e.g (Wang et al., 2013).), specifically suggesting that the importance of one over the other process might be highly site dependent. Recently, research shifted to the importance of floc constituents such as mineral composition of sediment grains, or the nature of organic constituents such as algae or diatoms on flocculation processes (e.g (Chen et al., 2005; Fettweis and Baeye, 2015; de Lucas Pardo et al., 2015; Verney et al., 2011).). This lead to the insight that biological processes play an important role in determining maximum aggregate size and suggested biology driven seasonal differences in particle settling behavior (Fettweis and Baeye, 2015; Lee et al., 2012); This has interesting implications for large-scale and long-term estuarine sediment transport, for instance it was shown that the settling behavior of large flocs together with vertical mixing and resuspension are governing estuarine residual sediment transport (Van Leussen, 2011).

Regardless of the aforementioned progress in understanding flocculation behavior and its impact on particle settling, measuring particle settling and more specifically settling velocities in the field is still a highly challenging endeavor. Field measurement techniques range from using in-situ settling chambers (Fennessy et al., 1994), to video systems or floc cameras (Van Leussen, 2011; Manning et al., 2010) to optical and acoustic methods (Fugate and Friedrichs, 2002; Voulgaris and Meyers, 2004).

Our goal is to compare two *in-situ* methods measuring settling velocity estimates, specifically a “multi-angle optics” and “acoustic backscatter” technique. These two techniques were chosen because of their minimal impact on particle populations and turbulence field and their simplicity of deployment and application (Fugate and Friedrichs, 2002).

The “multi-angle optics” technique, using an in-situ scatterometer (specifically a Laser In Situ Scattering and Transmissometer henceforth referred to as LISST), emits a single frequency laser and subsequently detects the intensities of laser light scattered from suspended particles with a series of concentric ring detectors. These intensities of scattered light gathered by the ring detectors are then inverted to estimate particle size distributions (Agrawal and Pottsmith, 2000, Agrawal et al., 2008). Recent tests showed the efficiency of the LISST device to measure uni- and multimodal particle size distributions (Agrawal and Pottsmith, 2000). However since in reality primary particle populations are more complex than for instance simple sand grains with respect to the refractive indices and size distributions the inversion approach that was used constitutes an underdetermined problem and therefore renders the resulting particles size distributions as approximate (Fugate and Friedrichs, 2002). Other *in situ* methods such as video or photography techniques (Van Leussen, 2011; Manning et al., 2010) or *in situ* settling chambers (Fennessy et al., 1994) may also provide reliable results on particle size spectra. However they are either logistically difficult to deploy and linked to high computational efforts during post-processing (the former) or influence the ambient turbulence field potentially changing floc distributions (the latter) motivating our choice. The measured LISST particle size distributions were then used to calculate settling velocity estimates applying the adapted Stoke's law; settling velocity estimates will be further referred to as wsLISST (Mikkelsen and Pejrup, 2001).

The “acoustic backscatter” technique transmits pulses of sound which are scattered back by particles suspended in the water column. The intensity and Doppler-shift of the backscattered signal are recorded using an Acoustic Doppler Velocimeter further referred to as ADV (Lynch et al., 1994), wich provides high frequency measurements of velocity components in x-,y- and z-direction (u,v,w). Previous laboratory experiments have shown that ADVs can provide estimates of flow and turbulence within 1% of the actual value (Voulgaris and Trowbridge, 1998). The measured turbulent fluctuations can subsequently be used to calculate settling velocity estimates based on the Reynolds-flux method utilizing the turbulent fluctuations in the vertical velocity component (w) and SPM concentration (c) (for details refer to 2.3.1), further referred to as wsADV (Fugate and Friedrichs, 2002; Voulgaris and Meyers, 2004). The sediment concentration was measured using an optical backscatter (OBS) sensor, which measures the amount of light scattered back after being emitted by a light source adjacent to the detector. This method's sensitivity to different suspended particle size distributions was demonstrated previously, where at moderate concentrations (depending on particle populations and sensor type) the aggregates cross-sectional area of suspended particles

directly governs how much light is backscattered, thus effectively measuring total grain cross-sectional area per unit area rather than mass concentration. The dependence on particle size distributions can result in poor calibration relationships between optical instrument outputs and field obtained gravimetric analyzes in estuarine environments where size distributions vary over time. Given that concentrations stay moderate this can be mediated through *in situ* calibration of the sensor with sediment samples aiming to sample the range of different particle populations and concentrations representative for the period of deployment (e.g. Lynch and Agrawal, 1991; Fugate and Friedrichs, 2002).

We conducted an intensive short-term field campaign investigating flocculation dynamics and testing the applicability of two state of the art methods on providing in-situ estimates of settling velocities in an intertidal channel. Previous applications of these methods by Fugate and Friedrichs (2002), Voulgaris and Meyers (2004), Wang et al. (2013) and Yang et al. (2016) provided an inspiring first appraisal of the possibilities of these methods in non-stationary intertidal systems. Nevertheless, (1) the influence of along-channel gradients and their associated flux divergence as a cause for violating underlying assumptions of wsADV estimates, (2) and the influence of changing primary particle populations on wsLISST estimates, has not been identified yet. We compare high temporal resolution measurements and discuss robustness of provided settling velocity estimates based on the different underlying assumptions of each method.

2. Materials and methods

2.1. Field site and instrument setup

One short-term field campaign was carried out in the main channel of the Sieperda marsh (Dutch-Belgian border; see Fig. 1). Salinity in this long and narrow main creek varies between 10 PSU and 14 PSU. The tidal range at its intertidal mouth is 2.9 m (data not shown), whereas at a gauge station in the main channel of the Scheldt River adjacent to the field site it amounts to 5.5 m (Bath) (Van Rijn, 2010; https://waterinfo.rws.nl). Suspended sediment concentrations measured at this adjacent gauge station showed a long-term average of 75.8 mg l^{-1} (http://live.waterbase.nl).

From May 13–14 2015 two measurement stations were established along the main channel of the Sieperda marsh. Station1 was located at 540 m from the channel mouth (N 51° 21.135′, E 4° 13.059′) and Station2 was located 1200 m landward of Station1 at (N 51° 20.734′, E 4° 12.241'). At Station1 we deployed two ADVs (Acoustic Doppler Velocimeters; Nortek Vector, 6 MHz), an OBS (optical backscatter sensor; YSI type 6920 V2), a LISST (Sequoia Science LISST-100C), and two submersible pump intakes to sample suspended particulate matter (SPM). The ADVs were mounted sideways above one another at heights of 20 and 40 cm above the bottom (cmab) with a continuous sampling frequency of 32 Hz. The pump intakes were fixed at the same heights as the respective probes, while ensuring a minimum of interference with the ADV measurements. The LISST was installed at 20 cmab, adjacent to the ADV location in landward direction, and measured continuously at a sampling interval of 10 s. The OBS was installed 1 m upstream of the ADV location at a height of 20 cmab and set to measure continuously at 1 Hz. This measurement setup was chosen such that all the equipment measures the same particle populations with as little as interference as possible.

At Station2 velocity measurements were collected with an ADV (Nortek Vector, 6 MHz); turbidity measurements were conducted using an OBS (YSI 6600 V2) and water samples were collected using a submersible pump with an intake at the same height as the ADV and OBS. The ADV was mounted in the sediment with an upward looking probe at 20 cmab. It measured continuously with a sampling frequency of 32 Hz (for details and on overview of the measurement setup refer to Table 1). Measurements started simultaneously for all instruments at both locations, prior to submersion. The OBS at Station1 started 10 min after submersion due to a programming error.

2.2. Calibration of sensor data to SPM concentrations

2.2.1. Calibration to suspended matter concentrations

The acoustic backscatter strength (ABS) of the ADV was calibrated to SPM concentrations using a 2-step method: (1) OBS-SPM calibration, and (2) ADV-OBS calibration. Because for the ADV located 40 cmab at Station1, no OBS was available, so the ABS was directly calibrated with SPM samples.

2.2.2. OBS– SPM calibration

Prior to deployment the OBS signal was calibrated in the laboratory using a diluted Hach 4000 NTU (Nephelometric Turbidity Units) Formazin standard to measure NTU. The OBS signal (NTU) was averaged over time intervals stretching from 30 s before to 30 s after the time point when the *in situ* SPM sample was taken. A linear regression model was fitted on the *in situ* SPM concentrations (mg l^{-1}) over the OBS (NTU) values to estimate the regression parameters. Subsequently, the raw OBS signal was converted to SPM concentrations (SPM_{OBS}) using these regression parameters (Fig. 2).

2.2.3. ADV– OBS calibration

A new SPM time series (SPM_{OBS}) was constructed from the OBS-based SPM estimates by bin averaging over 1 min intervals (bins), centered around a sampling time, to increase the robustness of the calibration. The sampling times were taken at a 5 min interval. The acoustic backscatter strengths from the three beams of the ADV were averaged to one average acoustic backscatter value (ABS) using the same temporal bins. These aggregated time series (SPM_{OBS} and ABS) were used to perform a log-linear regression in which the SPM_{OBS} data were log-transformed. In contrast to other studies (e.g (Voulgaris and Meyers, 2004).), the ABS signal was not log-transformed. For Nortek ADV sensors this log-transformation is already accomplished within the equipment's internal logarithmic AD-converter (i.e. ABS is in fact log(Intensity)) (Salehi and Strom, 2010). Subsequently, the regression model was used to convert the beam averaged ABS data to a SPM_{ADV} time series (in mg/l; and a frequency of 32 Hz).

2.2.4. ADV– SPM calibration

The ADV at Station1 (40 cmab) was directly calibrated to SPM concentrations using SPM water samples. A binning approach similar to that for the OBS-SPM calibration (see 2.2.2) was used combined with a linear regression to corresponding log-transformed SPM concentrations (Fig. 2).

Measurements during emersion were removed through post-processing. SPM sampling started from the moment the ADV probes and their measurement volumes were completely submerged. SPM samples were taken approximately every 15 min. SPM samples were taken with hand bilge pumps through hoses with intakes located at the OBS and ADV probes. The hoses had an internal diameter of 1.2 cm and a length of 5 m. Two minutes prior to each sampling, pumping was started to exclude residual water from the previous sampling. After 2 min of flushing, 1 L of water sample was taken. SPM samples were collected in PE containers in the field, covered, transported and subsequently analyzed in the lab. SPM concentrations were determined by filtration over pre-combusted 1.2 μm pore size glass fiber filters (Whatman GF/C). Three SPM

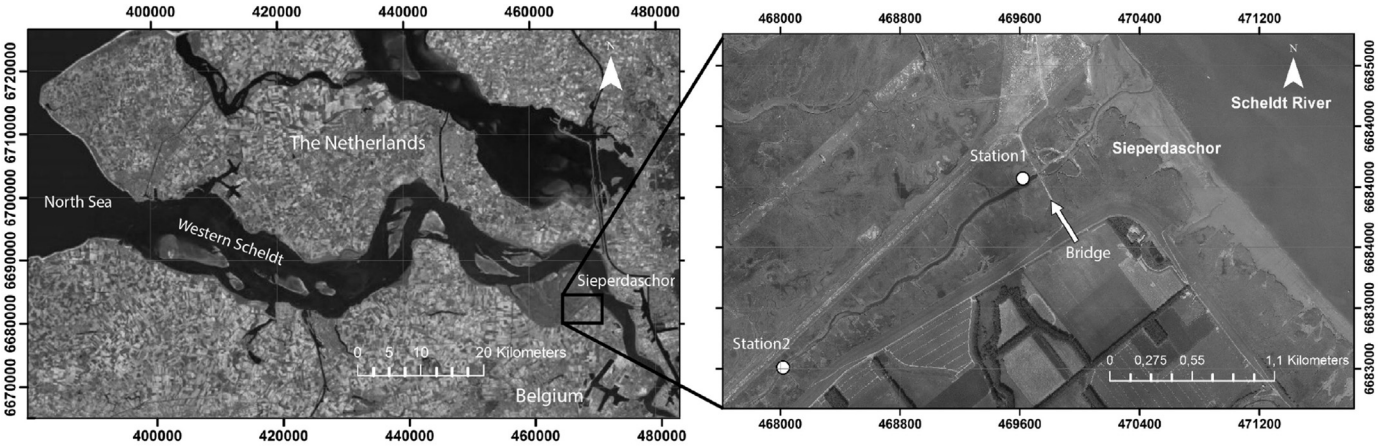

Fig. 1. (left) Overview of the Scheldt estuary; (right) overview of the measuring site, i.e. the main channel of the Sieperdaschor salt marsh located in the brackish zone of the estuary; Station1 and Station2 constitute the two measurement locations, of which Station1 is adjacent to a channel constriction at a bridge (indicated by an arrow); the coordinate system is Amersfoort, EPSG:28992.

Table 1
Overview of the field measurement setup.

Instrument	Details	Elevations (cmab)	Sampling details
Station1			
ADV	Nortek 6 MHz ADV	20, 40	Meas. Interval: 32 Hz
OBS	YSI 6920 V2	20	Meas. Interval: 1 s
Water pump		20, 40	
LISST	Sequoia LISST-100C	20	
Station2			
ADV	Nortek 6 MHz ADV	20	Meas. Interval: 32 Hz
OBS	YSI 6600 V2	20	Meas. Interval: 1 s
Water pump		20	

samples were analyzed for grain size distribution (Malvern Master Sizer, 2000) after being placed for 180 s in an ultrasonic-bath. This was done for 3 samples at Station1, at maximum flood, high water slack and maximum ebb.

2.3. Settling velocity estimation

Two commonly used methods for *in-situ* determination of particle settling velocities were used in this study: (1) wsADV based on the Reynolds-flux method (Cartwright et al., 2013; Fugate and Friedrichs, 2002; Voulgaris and Meyers, 2004) and (2) wsLISST based on the adapted Stokes' law following (Winterwerp, 1998).

2.3.1. Reynolds-flux method (wsADV)

The Reynolds-flux method estimates the settling velocity (w_s) based on direct observations of turbulent fluctuations in vertical velocity (w) and SPM concentration. By definition, the vertical turbulent flux, or Reynolds-flux, is given by $\langle w' c' \rangle$, where w' and c' are the turbulent fluctuations of vertical velocity, w, and SPM concentration, C, and <.> denotes Reynolds-averaging. Subsequently, if a first order balance between gravitational settling and vertical turbulent dispersion can be assumed, the settling velocity can be estimated as (Cartwright et al., 2013; Fugate and Friedrichs, 2002):

$$w_s = \frac{w' C'}{C} \tag{1}$$

In practice, the Reynolds averages are approximated by a time average over a chosen averaging period (here 5 min). Hence all quantities in (1) can be calculated from the calibrated ADV time series: w' and C' are the residuals after averaging of instantaneous vertical velocity and sediment concentrations, and $< C >$ is the average sediment concentration estimated from the ADV acoustic backscatter strength data (SPM_{ADV}). The Reynolds-flux method of estimating settling velocities has been applied in laboratory (Toorman, 2002, 2003) and field settings (Fugate and Friedrichs, 2002; Voulgaris and Meyers, 2004).

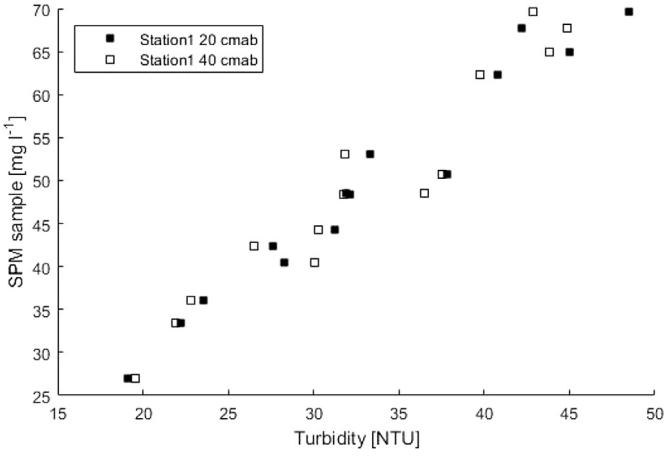

Fig. 2. Calibration curve between optical backscatter measurements (OBS) and collected SPM samples at Station1 of the main channel of Sieperdaschor; black squares show the lower position (20 cm above bottom); white squares show the higher position (40 cm above bottom); with SPM = 6.626 + 1.385 × Turbidity, $R^2 = 0.93$.

$$w_s = \frac{w' C'}{(C - C_{wash})} \tag{2}$$

However previous literature (Cartwright et al., 2013) indicates that the ADV responds to two distinct non-interacting particle size classes: a population of large (fast settling) flocs and a stable background population of smaller (non-settling/neutrally buoyant) particles. Cartwright et al. (2013) argued that only the concentration of fast settling flocs contributes appreciably to the Reynolds-flux, which makes it necessary to subtract the concentration of the non-settling background population ("washload", C_{wash}, equation (2)) from the measured average sediment concentration <C> to get a robust settling velocity. The concentration of C_{wash} was set

to the minimum SPM concentration observed during high water slack following Cartwright et al. (2013). Recent studies show the applicability of this method throughout different field situations, supporting its relevance for settling velocity estimates in the field (Brand et al., 2010; Wang et al., 2013; Yang et al., 2016).

Before calculating turbulent fluctuations, the raw data was pre-processed to remove observational artifacts as follows. ADV velocities and backscatter were de-spiked following the method by Vickers and Mahrt (1997). To ensure that the main current direction (u) corresponds to the x-direction, double axis rotations (rotation around the transversal (v) and vertical axis (w) (Lorke et al., 2013; Wilczak et al., 2000); were performed on all velocity data. This prevents that sensor misalignment with the main current direction can influence settling velocity estimates. Subsequently turbulent fluctuations where computed in successive 5 min intervals (bursts) as the residuals of a linear trend fitted through the de-spiked and rotated observations. All signal processing was performed in the R Statistical Software (R_Core_Team, 2013).

2.3.2. Adapted Stokes' equation (wsLISST)

Particle size distributions (PSDs) were measured with the Sequoia scientific laser in-situ scattering and transmissiometry instrument (LISST − 100C, range 2.5–500 μm).

The settling velocity of spherical particles can be described by Stokes' Law, under the assumption that the particle Reynolds number is smaller than one. Aggregates (flocs) that are formed in suspensions of cohesive sediment have irregular shapes and non-uniform density. For such flocs the settling velocity becomes an intractable function of the particle shape and density distribution. Importantly, larger flocs tend to be more loosely bound and to have a lower density compared to smaller more tightly packed flocs, resulting in decreasing effective density with increasing floc size. Thus, estimates of settling velocities can be derived only if the relationship between effective density and floc size is established. This has been done by, assuming self-similarity between primary particles and flocs based on fractal theory (Winterwerp, 1998) and by using density functions that describe the mass distribution over the PSD (Markussen and Andersen, 2013). It is important to recognize that the PSD measured by the LISST represents a bulk particle size distribution including both settling and non-settling populations.

Here we calculated settling velocities using the adapted Stokes' equation (Lee et al., 2012; Winterwerp, 1998):

$$w_s = \frac{(\Delta\rho)g}{18\mu} D_p^{3-nf} \frac{D^{nf-1}}{1 + 0.15Re^{0.687}} \tag{3}$$

$$Re = \frac{w_s D}{\upsilon} \tag{4}$$

where w_s (mm s^{-1}) is the settling velocity; the effective density ($\Delta\rho$) (kg m^{-3}) was calculated as the quotient between the OBS measured suspended particulate matter concentration (SPM_{OBS}), and the floc volume concentration measured by the LISST, (VC) (Mikkelsen and Pejrup, 2001; Voulgaris and Meyers, 2004). The size of primary individual particles (D_p) (m) was set as 10 μm, the average primary particle size measured with a Malvern mastersizer during maximum flood, high water slack and maximum ebb. The fractal dimension of the suspended particles (*nf*) was calculated, by fitting a linear regression using the least-squares method for the relationship between $\Delta\rho$ and D_p. Specifically the fractal dimension equals 3 minus the slope of the regression line (Hill et al., 1998; Mikkelsen and Pejrup, 2001). D represents the median floc diameter (D_{50}) measured by the LISST, with μ the molecular viscosity and υ the kinematic viscosity.

LISST data was collected continuously every 10s for one day of diurnal tide. Good data quality for the LISST was assumed if optical transmission was between 15% and 98%, and no gradual or sudden increase or decrease in transmission or volume concentration occurred.

2.3.3. Shear rate estimates

The effect of turbulence on floc formation can be determined by the shear rate (G), which depends on the turbulence dissipation rate (ε) following (Dyer and Manning, 1999; Van Leussen, 2011):

$$G = \left(\frac{\varepsilon}{\upsilon}\right)^{1/2} \tag{5}$$

with

$$\varepsilon = \frac{u_*^3}{\kappa z} \tag{6}$$

where υ represents the temperature corrected kinematic viscosity (0.96×10^{-6} m^2 s^{-1}), κ is the "von Karman" constant (0.41), z is the height above bed of the sensor (m), and u_* is the shear velocity (m s^{-1}), which can be determined using the Reynolds stress corrected for the sensor height following (Voulgaris and Meyers, 2004)

$$u_* = \sqrt{-\overline{u'w'}} \tag{7}$$

where u' and w' represent turbulent fluctuations, calculated as residuals after burst averaging horizontal and vertical current respectively.

3. Results

3.1. Hydrodynamics and suspended material concentrations

Hydrodynamic measurements conducted with ADVs show a clearly flood-dominated asymmetry in the horizontal tide (Fig. 3a–f). At Station1, a maximal horizontal flood velocity (20 cmab) of 0.46 m s^{-1} and a maximum horizontal ebb velocity of 0.35 m s^{-1}, with a maximum water depth at high water slack of 2.41 m was found (Fig. 3e). At Station 2 we observed a maximum flood velocity (20 cmab) of 1.01 m s^{-1} and a maximum ebb velocity of 0.65 m s^{-1}, with maximum water depth at high water slack of 2.58 m (Fig. 3f). Both stations exhibit a clear flood dominant tidal asymmetry, with a more pronounced flood dominance at Station2 (Fig. 3a–d).

SPM_{OBS} concentrations (20 cmab) exhibit a clear variation between the ebb and flood tidal stage, at Station1 showing a maximum flood SPM_{OBS} concentration of 76.2 mg l^{-1} and a maximum ebb SPM_{OBS} concentration of 51.5 mg l^{-1} (Fig. 3c). At Station2 we observe a maximum flood SPM_{OBS} concentration of 105.0 mg l^{-1} and a maximum ebb SPM_{OBS} concentration of 79.6 mg l^{-1} (Fig. 3d). SPM_{OBS} concentrations at high water slack vary between 35.6 mg l^{-1} and 36.8 mg l^{-1} at Station1 and 38.2 mg l^{-1} and 41.5 mg l^{-1} at Station2. Tidal averaged SPM_{OBS} concentrations vary between 43.6 and 46.5 mg l^{-1} and at Station1 and 51.2 mg l^{-1} and 61.2 mg l^{-1} at Station2 over the measured semi-diurnal tidal cycle (Fig. 3c and d).

The particle size distributions as measured by the LISST at Station1 showed a clear variation over the tidal cycle; as the instrument did malfunction during the second diurnal tide, we only show data from the first measured tide (Figs. 4 and 5).

Around the moment of peak flood velocity (blue plane, Fig. 4; Fig. 5b) we observe a peak at low particle size distributions (low mean particle diameter) and high suspended sediment

concentrations. As the tidal cycle progresses, horizontal velocities and concentrations decrease reaching their minimum around high water slack. During this period concurrent steady increase in coarse particle sizes accompanied by a reduction in fine particle sizes is observed leading to a maximum particle size of 190 μm at high water slack when flow velocity is minimal (green plane, Fig. 4; green bars Fig. 5b). As the ebb tidal cycle proceeds and velocity increases again, a reduction in coarse particle sizes occurs accompanied by an increase in fine particles size, reaching a minimum in particle sizes at maximum ebb velocity (red plane, Fig. 4; red bars Fig. 5b). Following maximum ebb velocity suspended sediment concentrations continue to increase with decreasing current velocities, leading at first to a continued increase in particle sizes, which ultimately decreases after the suspended sediment fell below 36 mg l^{-1} concentration (Figs. 4, 5b and 7a).

A comparison between the *in-situ* measured particle size distributions (LISST) and measured particle size distributions in the laboratory, after mechanical destruction of flocs, reveals clear differences at the indicated time points (peak flood, high water slack, and peak ebb) (Fig. 5). Laboratory samples represent the sizes of the primary unflocculated particles, as they are mechanically disaggregated through sonication and show only little variation in D_{50} over the measured tide, ranging from 9.1 μm (at peak flood), 11.3 μm (at high water slack) and 9.7 μm (at peak ebb) (Fig. 5a blue, green and red bars). In contrast, particle size distributions measured with the LISST show a clear variation over the measured tide ranging from 54.7 μm (at peak flood), 189.9 μm (at high water slack) and 71.2 μm (at peak ebb) (Fig. 4 blue, green and red line respectively, Fig. 5b).

Our measurements indicate a negative relationship between *in-situ* measured median particle or floc diameter and the Shear Rate G over the largest part of the tidal cycle. A detailed analysis of the variation in median diameter as a function of shear rate reveals a counter-clockwise hysteresis in mean floc diameter during ebb tide, while a less pronounced hysteresis during flood (Fig. 6a). However, during the first part of flood and the final part of ebb, this negative correlation and observed hysteresis is not present (Fig. 6a). We further observe a hump-shaped relationship between measured mean particle/floc diameter and SPM concentration over the whole tidal cycle. A separate comparison between ebb and flood cycles shows that median particle diameters during ebb seem to be positively correlated with SPM concentration, whereas at flood the opposite (negative correlation) is the case (Fig. 6b). We further see a clear asymmetry in current velocity between ebb and flood – tide (Fig. 6c).

3.2. Settling velocity estimates

Although settling velocities estimated from the ADV (wsADV) and LISST method (wsLISST) exhibit a comparable range (Fig. 7), they reveal a clear difference in tidal variation (Fig. 7a). Around the flood and ebb maxima, the wsADV estimates are highest, whereas

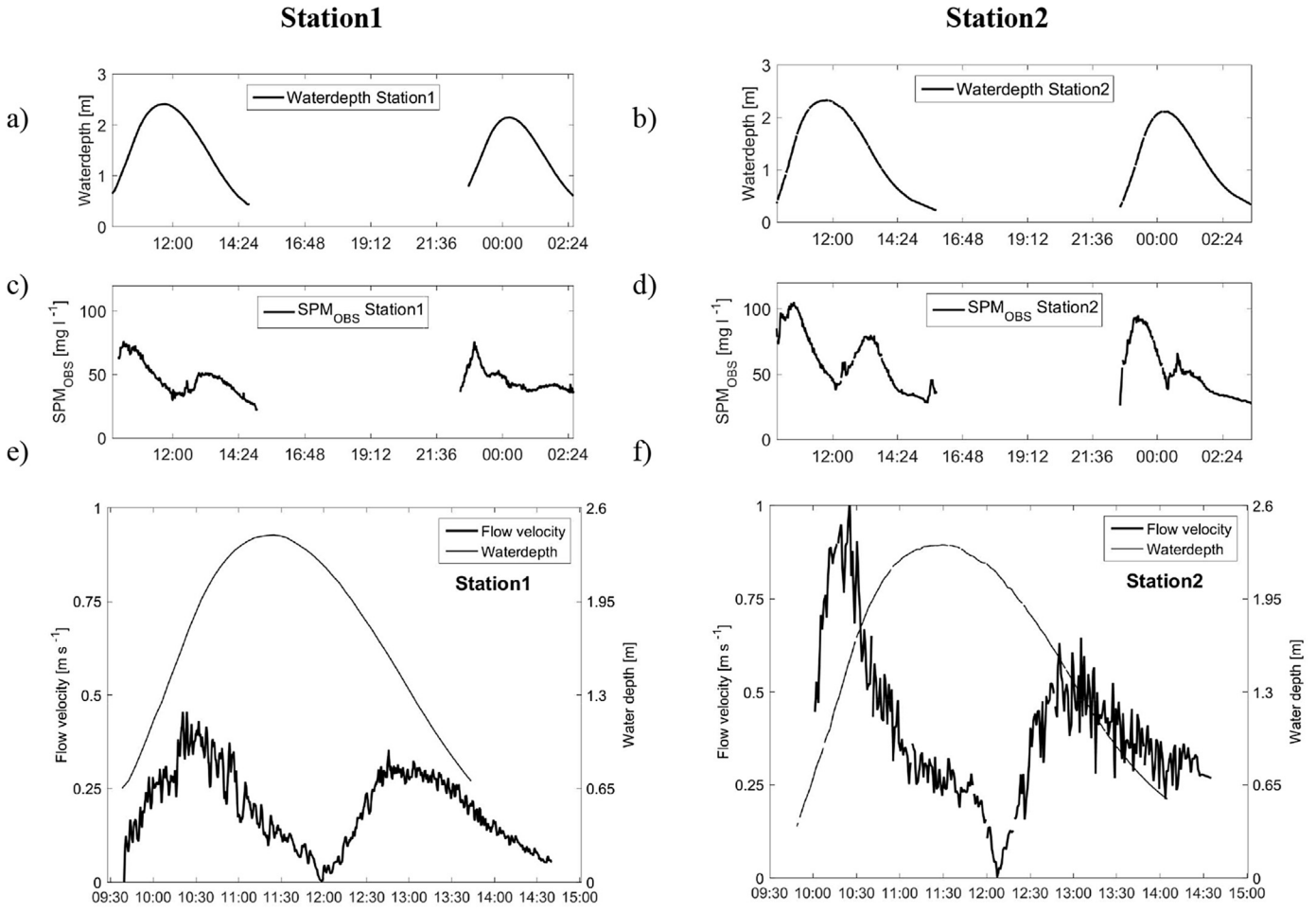

Fig. 3. Time series of measured (a) water depth, (c) SPM, and (e) water depth and velocity of the first semi-diurnal tide at Station1 and of (b) water depth, (d) SPM and (f) water depth and velocity of the first semi-diurnal tide at Station2.

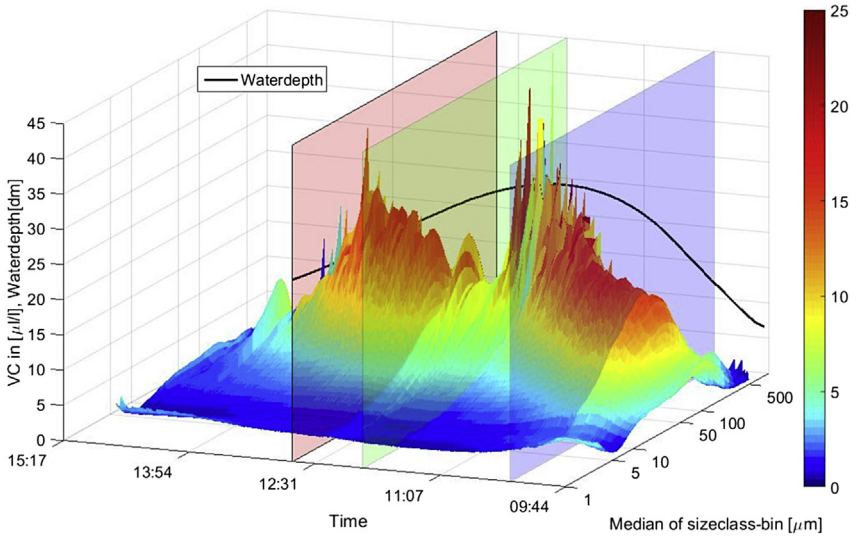

Fig. 4. Volume concentrations (VC) per particle size class(plotted by the median of each size class) over one tidal cycle measured by the LISST; the colorbar indicates volume concentrations in [µl/l]; the z-y plane in the back of the graph shows water depth over time in [dm]; the three colored planes indicate from right to left: (blue) maximum flood velocity, (green) high water slack, (red) maximum ebb velocity. (For interpretation of the references to colour in this figure legend, the reader is referred to the web version of this article.)

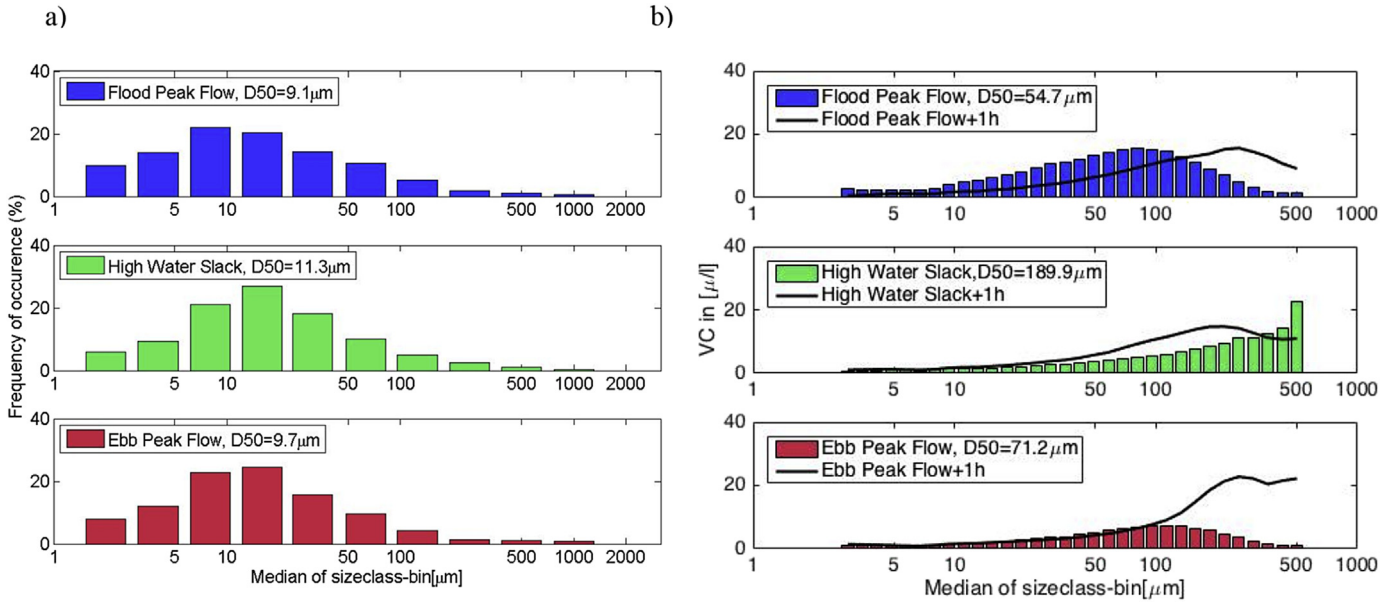

Fig. 5. Comparison of PSDs measured in the lab (a) with a Malvern Master Sizer (2–2000 µm) and *in-situ* (b) with a LISST (2.5–500 µm) over the measured tide, black lines show the particles size distribution after an additional hour from the indicated time points. Colors of the PSD match vertical lines in Fig. 7 and vertical planes in Fig. 4, from top to bottom: (blue) maximum flood velocity, (green) high water slack, (red) maximum ebb velocity. (For interpretation of the references to colour in this figure legend, the reader is referred to the web version of this article.)

wsLISST estimates are lowest (Fig. 7a, blue and red line), and vice versa. A comparable temporal variation of wsADV estimates with flow velocity can be observed, with high values of wsADV at maximum ebb and maximum flood (Fig. 7c, blue and red line) and low values at high water slack (Fig. 7c, green line). Suspended matter concentration (SPM_{OBS}) seems to follow a similar temporal variation shifted by a time lag (Fig. 7c).

To allow a comparison between settling velocity estimates (wsADV) of the top and bottom ADV sensor at Station1 between both tidal cycles, the estimates from the second cycle have been time shifted for 12.4 h to align them (Fig. 8). A clear temporal pattern can be distinguished: the wsADV estimates show maxima during the initial phases of both flood and ebb. The maximal wsADV estimate during flood (0.9 mm s^{-1}) is recorded with the bottom sensor, while the maximal wsADV estimate during ebb (2.4 mm s^{-1}) is recorded with the top sensor. After reaching their maximal values, the wsADV estimates decrease towards the end of both flood and ebb phases. During high water slack, the wsADV estimates are close to 0 mm s^{-1}, while wsADV estimates are always non-zero at the end of ebb. Further, settling velocity estimates during ebb are consistently higher than during flood. This overall pattern is most consistent at the bottom sensor. Particularly during ebb phase, the estimates at the top sensor show variable behavior; e.g. during the last 40 min of the first cycle the wsADV estimates

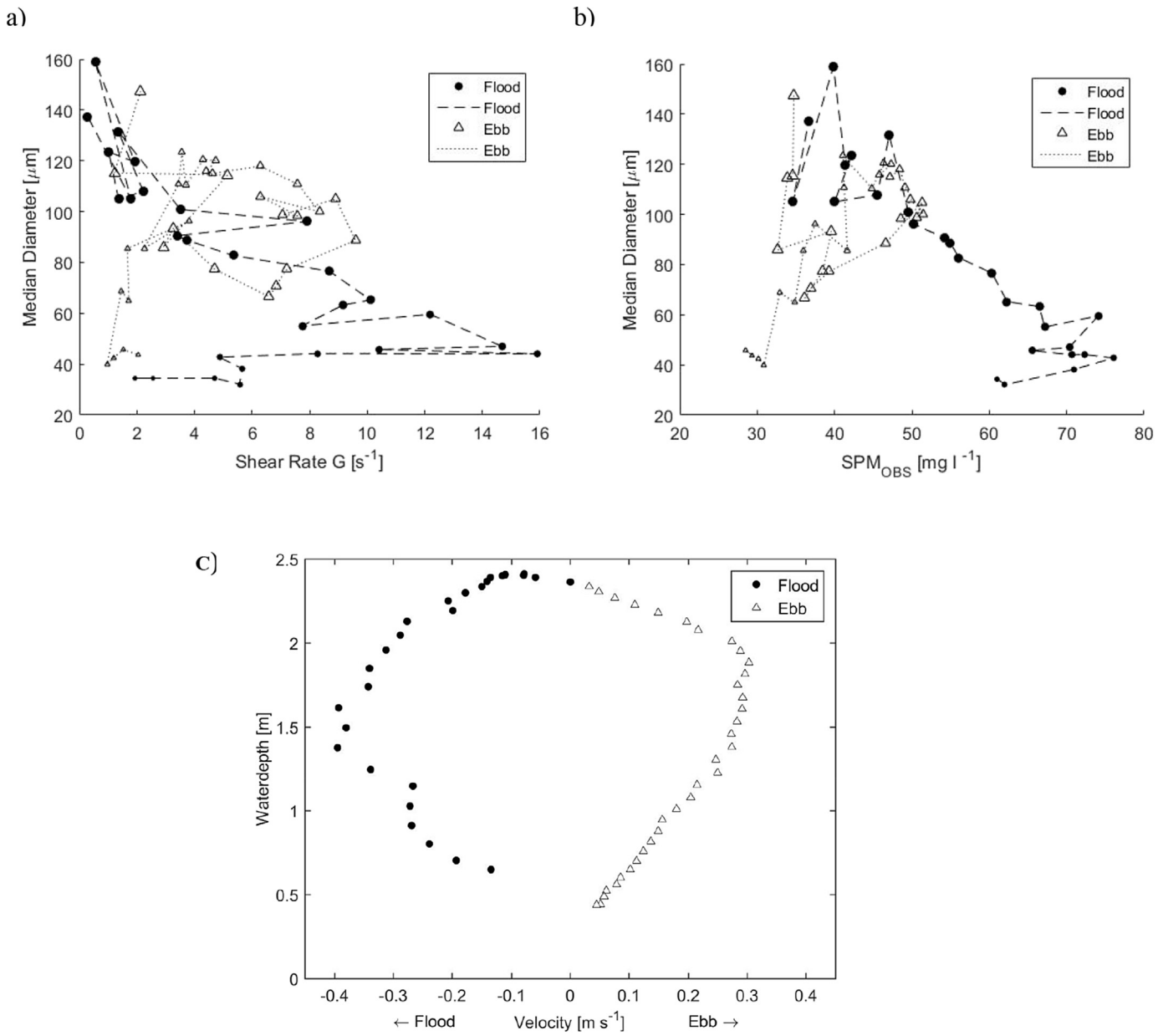

Fig. 6. Relationship between (a) median) floc diameter and shear rate (G); (b) Relationship between median floc diameter and SPM concentration; symbol size scales with water depth, black symbols and dashed lines represent the flood phase, white symbols and dotted line represent the ebb phase.

increase, while during the last 60 min of the second tidal cycle they fluctuate. Note that the first tidal cycle has overall higher water levels than the second cycle, resulting in a longer period of inundation of the sensor and thus longer time series of settling velocity estimates.

4. Discussion

A comparison between settling velocity estimates measured at two different sites in an estuarine creek and with two different methods reveals clearly different estimates over a semi-diurnal tide. Settling velocity estimates conducted with the Reynolds-flux method (wsADV) show temporal variations that are comparable between the two stations (data not shown), whereas the temporal variations observed at Station1 differ when compared between the different methods, i.e. wsLISST and wsADV. In the following discussion we critically assess assumptions underlying both methods and use this analysis to explain the observed discrepancy between the methods.

4.1. Settling velocity estimates: similarities between Reynolds-flux method and the adapted Stoke's method

Settling velocities estimated through the Reynolds-flux method (wsADV) are based on turbulent fluctuations of suspended sediment concentrations. Whereas settling velocity estimates based on the adapted Stokes' law (wsLISST) following (Winterwerp, 1998), mainly scale with the temporal variation in floc size (D_{50}) as measured with a LISST (Figs. 4, 6 and 7).

As shown in (Fig. 7a and b) temporal variations of settling velocities estimated with the Reynolds-flux method (wsADV) are negatively correlated compared to estimates calculated from the

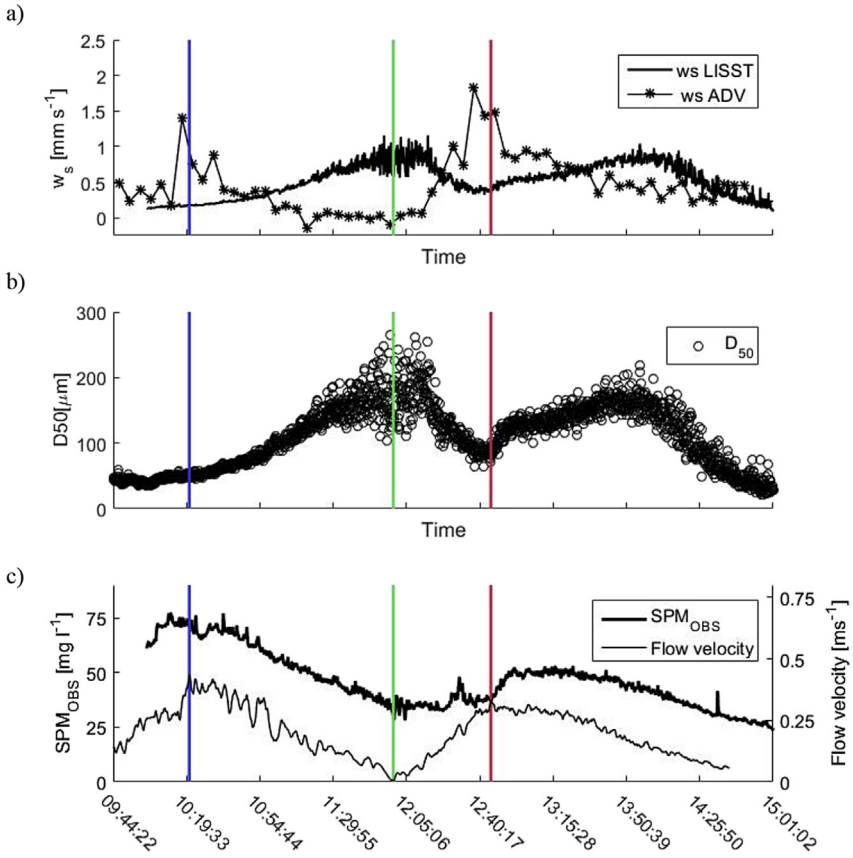

Fig. 7. Comparison of the temporal variation in settling velocity estimates (a) between wsLISST and wsADV, (b) D50 over time; (c) SPM_{OBS} and flow velocity over the measured tide; the three colored lines indicate from left to right: (blue) maximum flood velocity, (green) high water slack, (red) maximum ebb velocity; the shorter SPM_{OBS} time series is due to a deployment error. The OBS at Station1 only started measuring at 10°. clock explaining these time series. (For interpretation of the references to colour in this figure legend, the reader is referred to the web version of this article.)

modified Stokes' method (wsLISST). This contrasts with previously reported flume measurement showing high correspondence between Reynolds-flux and Stokes' method (Toorman, 2003, 2002).

Recent studies show comparable temporal variations in floc size distributions and therefore also settling velocity estimates based on the Stokes' method (wsLISST) over the tidal cycle (Fettweis and Baeye, 2015; Hill et al., 2013). We hence hypothesize that observed discrepancies in temporal variation of settling velocity estimates between the two methods can be explained from underlying assumptions of the Reynolds-flux method. To address this hypothesis we revisit the original derivation of the Reynolds-flux method to address the causes for this apparent contradiction in our particular case.

In a straight channel with zero bottom slope and constant cross-section, the Reynolds averaged continuity equation for suspended sediment can be approximated as (Fugate and Friedrichs, 2002; Voulgaris and Meyers, 2004).

$$\frac{\partial\langle C\rangle}{\partial t} + \frac{\partial(\langle u\rangle\langle C\rangle)}{\partial x} = w_s\frac{\partial\langle C\rangle}{\partial z} - \frac{\partial}{\partial z}w'C' \tag{8}$$

where the z-axis is pointing upwards, C is the SPM concentration, u horizontal velocity, w vertical velocity, w_s is the settling velocity as a positive scalar, and $< . >$ denotes Reynolds averaging. Under stationary conditions, i.e. no concentration change over time or length axis, a balance exists between the two terms on the right hand side of the equation: upward turbulent transport (second right-hand

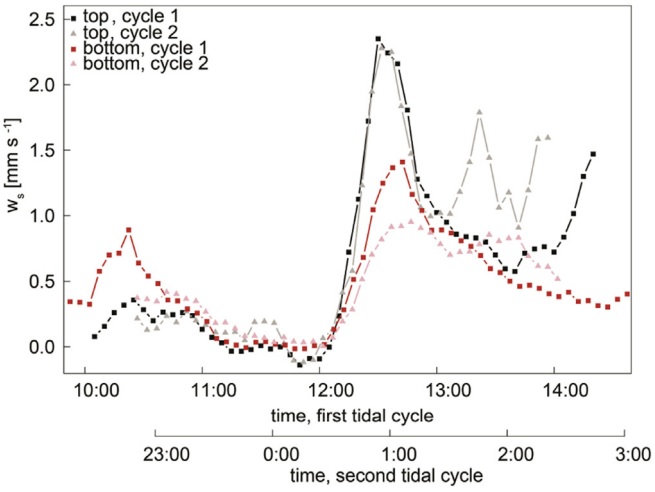

Fig. 8. Comparison of settling velocity estimates at Station1 between top ADV (grey and black lines for 2 tidal cycles) and bottom ADV (red and light red lines for the same 2 tidal cycles), smoothed with a moving average filter (symmetric block-type, N = 4). Estimates from the second tidal cycle have been time shifted for 12.4 h to be able to plot the data on the same time axis. (For interpretation of the references to colour in this figure legend, the reader is referred to the web version of this article.)

side term) equals gravitational settling (first right-hand side term). After vertical integration of the SPM concentration between the bed and the sensor height, equation (8) is retrieved provided that there is no sediment flux to or from the bed.

Field conditions however violate these assumptions as channels have a more complex geometry and experience non-stationary sediment flux conditions. The Reynolds-flux method assumes that the continuity equation is predominantly governed by the aforementioned vertical balance. When the terms on the left-hand side of equation (8) are not zero, they should at least be sufficiently small to be neglected. Researchers have justified this assumption with complementary measurements or order of magnitude calculations. For instance, Fugate and Friedrichs (2002) estimated the local change term (term1 in equation (8) by SPM measurements at different heights and estimated along channel advection of SPM (term2 in equation (8)) through different measurements of SPM concentrations at different points along the channel. These terms appeared to be an order of magnitude lower than the settling term (term3 in equation (8)) and can then be safely neglected. Voulgaris and Meyers (2004) estimated the local term (term1 in equation (8)) from ADV-derived sediment concentrations and for the 2nd term they assumed that the velocity diminishes to zero at the landward end of the channel and that the SPM at the most upstream channel end is equal to the minimum values observed at the measuring station. As such, the horizontal gradient (term2 in equation (8)) values were 3–5 orders of magnitude smaller than the measured settling term. Other researchers have directly compared the Reynolds-flux method with other *in-situ* techniques (Cartwright et al., 2013): for instance used Particle Imaging Camera System to estimate settling velocities over half a tidal cycle in an *in-situ* settling-column. They found a good correspondence over the largest part of the cycle, although they stressed the importance of the wash-load (non-settling population).

It is however very important to realize that these justifications are site-specific and strongly dependent on the prevailing hydrodynamic conditions. We argue that in our case the governing equilibrium assumptions are temporarily not fulfilled, leading to the observed mismatch in settling velocity estimates from the adapted Stoke's (wsLISST) and Reynolds-flux method (wsADV). Specifically, we attribute the mismatch to two phenomena; (1) the presence of transient vertical fluxes during accelerating and deceleration flow, and (2) the importance of horizontal flux divergence.

4.1.1. Vertical sediment fluxes during transient flow (wsADV)

An imbalance between upward turbulent transport and gravitational settling results in vertical redistribution of suspended particles over the water column. There are two dominant conditions in tidal systems when we can expect such redistribution. First, during accelerating (respectively decelerating) flow, the turbulent diffusivity will increase (respectively decrease) causing an upward (respectively downward) redistribution of particles. Thus, over a tidal cycle, these alternating periods of upward and downward redistribution of particles, results in Reynolds-flux being larger (respectively smaller) than gravitational settling. Second, during periods of erosion from or deposition on the bed, the concentration of particles in suspension changes. Since the exchange with the bed is a local process, this will also imply a vertical redistribution of particles over the water column. Thus we expect that the Reynolds-flux is larger than gravitational settling during periods of erosion/accelerating flow, and lower during periods of deposition/decelerating flow. In summary.

$w'C' = w_sC$ stationary conditions.
$w'C' > w_sC$ accelerating flow and/or erosion.
$w'C' < w_sC$ decelerating flow and/or deposition.

To see what the corresponding effects are on the vertical gradients of particle concentration, we adopt a turbulent diffusivity model for the Reynolds-fluxes:

$$A_z\frac{\partial C}{\partial z} \equiv w'C' \tag{9}$$

with A_z as the turbulent diffusivity.

As shown above, equilibrium assumptions of a vertical balance between upward turbulent diffusion and gravitational settling are not likely to be fulfilled over the whole tidal cycle. We hypothesize that this is mainly due to acceleration/deceleration effects leading to temporary non-equilibrium states as described by Holtappels et al. (2013) for oxygen flux measurements. This hypothesis is supported as we find a close relationship (though with a certain time lag) between, on the one hand, the difference in settling velocity estimates wsLISST and wsADV, and on the other hand the magnitude of flow acceleration and deceleration processes (Fig. 9).

4.1.2. The importance of horizontal flux divergence (wsADV)

We assess the existence of a first order balance between turbulent mixing and gravitational settling in our field situation by evaluating the terms of the sediment continuity based on measured field data (4.1.2.1) and scaling arguments (4.1.2.2). By comparing magnitudes of the Reynolds-flux and gravitational settling with the remaining terms of the sediment continuity equation we can assess the impact of the local term and the advective term (horizontal flux divergence) on the reliability of the wsADV settling velocity estimate.

4.1.2.1. Estimating the various terms in the continuity equation. To assess whether assumed equilibrium conditions are met in our case we use our data set to estimate terms of the sediment continuity equation (equation (8)) to evaluate whether some terms can indeed be neglected as assumed by the Reynolds-flux method.

We estimated the advective term (term2 in equation (8)) (Fig. 10d) in two ways. Firstly, using only local data, we applied the sediment continuity equation (equation (8)) and filled in the settling term ($ws \times dC/dz$; estimated from the LISST, Fig. 10a), the Reynolds-flux term ($d < w'C'>/dz$; estimated from the ADV, Fig. 10b) and the local term (dC/dt estimated from the OBS, Fig. 10c). Secondly, we calculated the difference in horizontal advection between Station1 and Station2 (specifically the vertical terms were calculated based on the two ADVs at Station1 mounted on top of each other, where the settling velocity in the settling term is calculated from the LISST).

From a relative comparison between the local term and both estimates of the advective term normalized by the settling term (Fig. 11), we see that for a large time range, neither the local term nor the advective term are small enough to be neglected, since they are in the same order of magnitude as the settling term. Overall the advective term is larger than the local term (Fig. 10c and d). It is further visible form local and longitudal estimates that the magnitude of the advective term is biggest at peak flow velocities (Fig. 10d). Further the local and longitudinal estimates of advection globally agree (Figs. 10d and 12): they exhibit the same order of magnitude however the detailed temporal variation is not consistent. We hypothesize that this is due to; (1) equating differences in u × C over a converging channel distance of 1.2 km to local gradients is a coarse approximation, (2) this approximation is not based on a mass balance constructed by averaging over the respective cross-section, but rather based on point measurements which make it difficult to interpret.

In summary we conclude that the left hand side of equation (8) is not negligible over long periods over the measured tide, which contradicts previous assumptions of the Reynolds-flux method.

4.1.2.2. Scaling arguments. Various researchers have used scaling arguments to motivate that a first order balance may be a good approximation for sediment transport, also in converging tidal channels (e.g (Friedrichs et al., 1998; Galappatti, 1983; Lanzoni and Seminara, 2002; Talke et al., 2009).). However, it was also noted that the longitudinal advective term (term2 in equation (8)) plays a delicate role, and is not as easily negligible as for instance the time varying term (term1 in equation (8)) and or dispersive flux terms (Friedrichs et al., 1998; Lanzoni and Seminara, 2002). These studies evaluated the scaling terms with typical values for sediment transport on the estuarine scale. Here we evaluate the scaling factors with values that are representative for our case study.

Adopting a turbulent diffusivity model, the non-dimensional equivalent of equation (8) reads (cf (Galappatti, 1983).)

$$\frac{H}{Tw_s}\frac{\partial c}{\partial t}+\frac{UH}{Lw_s}\frac{\partial (uc)}{\partial x}=\frac{\partial c}{\partial z}-\frac{K}{Hw_s}\frac{\partial}{\partial z}\left(k\frac{\partial c}{\partial z}\right) \quad (10)$$

where *T, H, L, U, K* are typical scale of time, water depth, length, horizontal velocity and vertical turbulent diffusivity. Following (Lanzoni and Seminara, 2002), time scales with the inverse of the angular frequency associated with the dominant tidal period are $T \sim 10^4$ s. From our observations we derive water depth, *H*, on the creek is in the order of ~1 m, horizontal velocity *U* ~1 m s^{-1} and *K* ~10^{-}3 m^2 s^{-1}. The length scale in the tidal creek is about L ~1 km. Settling velocity is of the order w_s ~10^{-3} m s^{-1}. Inserting these scales in equation (10) we see that the transient term (term1 equation (10)) is on the order 10^{-1}, but importantly the advective term (term2 equation (10)) is of the order 1, as are the vertical dispersive (term3) and the settling term (term4). Thus, in our case study, advective transport is of the same order as gravitational settling and turbulent dispersion.

In contrast, for estuarine settings (Talke et al., 2009), the scaling of the advective term is of the order 10^{-1} (for *H* to 10 m, *U* to 0.01 m s^{-1}, L to 10 km and *K* 0.001 m^2 s^{-1}). The contrast with our case study results from the dimensions of the tidal creek: both the depth and the characteristic length scale are much smaller compared to Talke et al. (2009). Thus, from scaling arguments we conclude that on the estuarine scale the first order balance is between vertical terms, whereas in a shallow tidal creek also advective terms and therefore horizontal flux divergence contributes in first order.

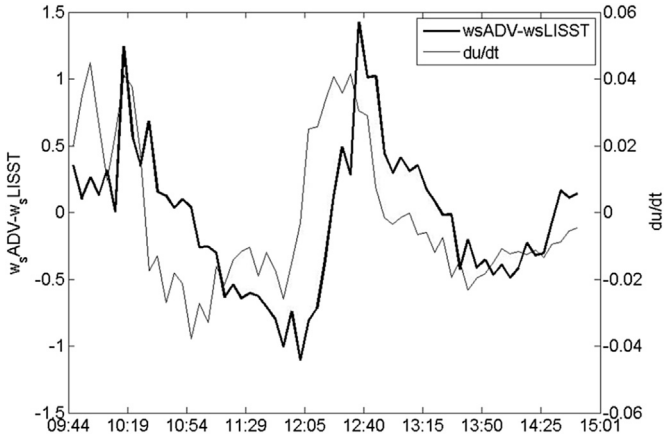

Fig. 9. Temporal variation of the difference in settling velocity estimates between the two employed methods (wsADV-wsLISST) and the magnitude of flow acceleration and deceleration (du/dt) at Station1 (20cmab). A similar temporal variation is visible shifted by a time lag.

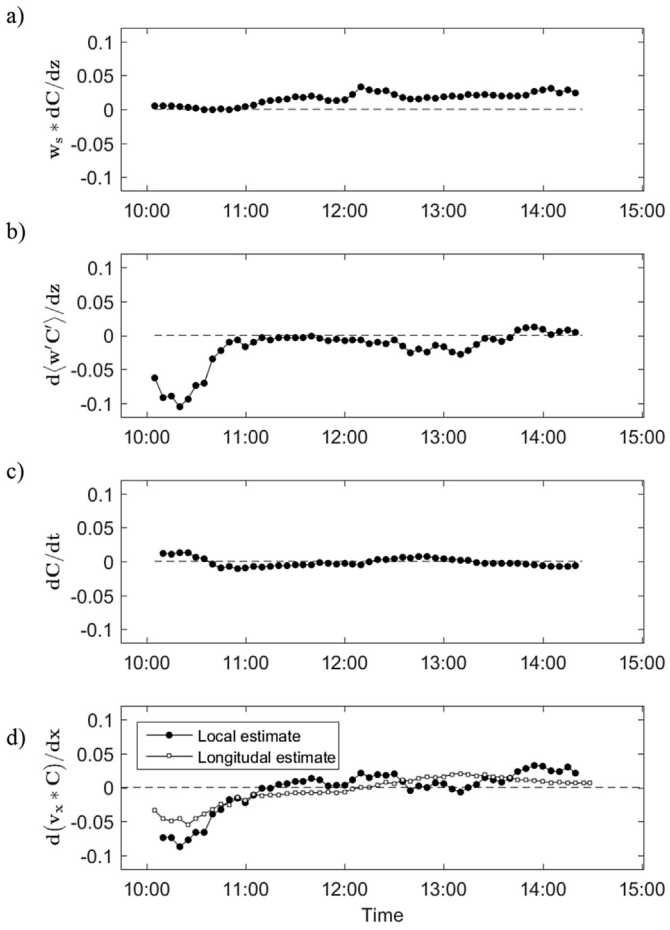

Fig. 10. Estimated transport terms of the continuity equation at Station 1: (a) the settling term was estimated using the LISST data, (b) the Reynolds-flux was estimated from calibrated turbulent fluctuations of the ADV measurements, (c) the local term was estimated through OBS estimated SPM concentration differences between top and bottom sensor at Station 1, (d) the advective term's local estimate was achieved by filling in the continuity equation (term a,b,c), the advective term's longitudal estimate was achieved by calculating horizontal advection between Station 1 and Station 2.

4.2. Flocculation effects (wsLISST)

4.2.1. Settling velocities estimates adapted Stokes' law (wsLISST)

To investigate uncertainties in temporal variation and magnitude of settling velocities estimated through the adapted Stokes' law following (Winterwerp, 1998), we tested its sensitivity to different primary particle populations. This was done by calculating settling velocity estimates (equation (3) and (4)) based on fractal dimensions and primary particles sizes of the whole particle population (average between ebb, flood and high water slack) and to particle populations measured at ebb, and flood separately (Fig. 12). Fractal dimension was determined by applying least square fitting routines between effective density (Δρ) and the measured D50 (both log transformed) for particle populations during ebb, flood and for the whole tidal cycle following (Mikkelsen and Pejrup, 2001) (Fig. 12a blue, red, black respectively). Primary particle sizes were measured during lab analysis of disaggregated field samples (Fig. 5). This resulted in a 33.8% lower settling velocity estimate using parameters of the ebb particle population and in a 53.4% higher settling velocity estimate using parameters of the flood particle population compared to the particle population during the whole tidal cycle. Nevertheless temporal variations in settling velocity estimates remained consistent (Fig. 12b).

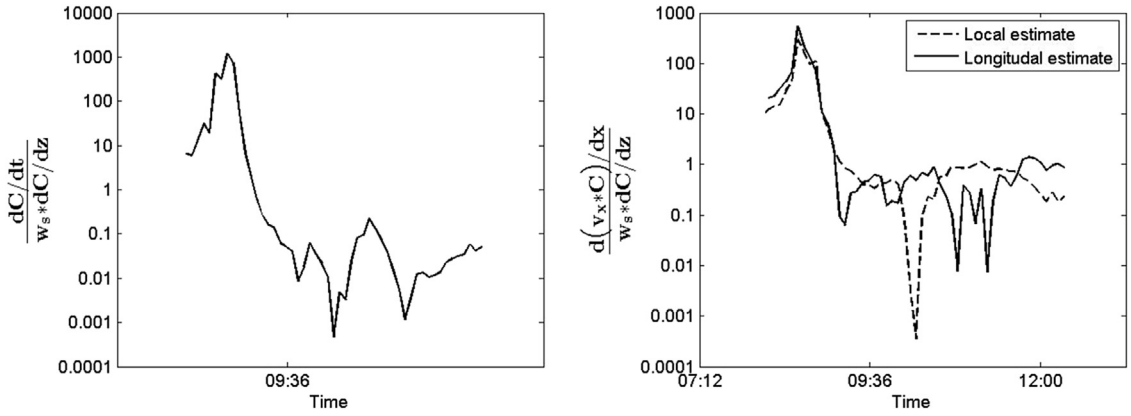

Fig. 11. Comparison of the relative importance of the local term (left) and the advective term (right) relative to the settling term over the measured tide. Shown is the tidal variability normalized over the settling term.

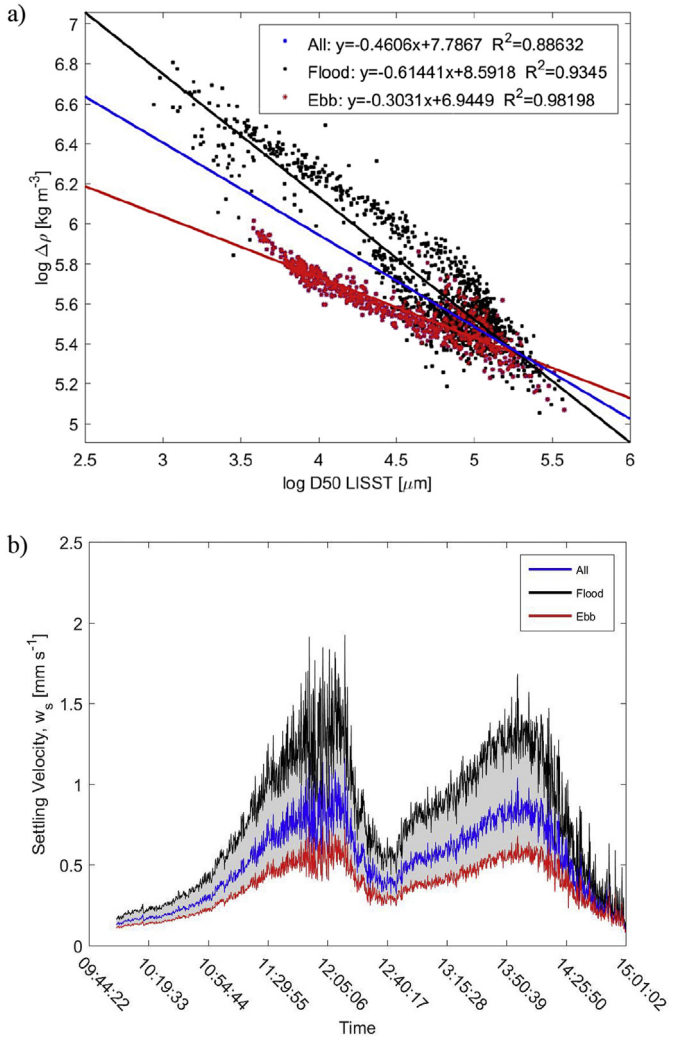

Fig. 12. (a) Least square fits determining the fractal dimension on particle populations at ebb (red), flood (black) and the whole tide (blue). (b) LISST settling velocity estimates using the adapted Stokes' law applied to particle populations over the whole tidal cycle (blue), ebb- (red) and flood (black) tidal phase. (For interpretation of the references to colour in this figure legend, the reader is referred to the web version of this article.)

4.2.2. Floc dynamics (wsLISST)

Flocculation in estuarine and marine environments is generally considered to be mainly governed by turbulence induced shear and SPM concentration. At low SPM concentrations flocs are small, but relatively low shear increases the likelihood of collision induced floc formation. This process is inverted with increasing shear, where the intensity of collisions can lead to floc break up. At higher SPM concentrations, larger floc sizes are present in quiescent water, which are however susceptible to disassociation through only a small amount of shear (e.g (Dyer, 1989, 1995; Hill et al., 2013; Safak et al., 2013; Wang et al., 2013).). These general flocculation principles are identifiable in the temporal variations in mean floc size measured by the LISST, which is in agreement with previously reported floc dynamics in intertidal systems (Figs. 4 and 5) (Fettweis and Baeye, 2015; Lee et al., 2012; Markussen and Andersen, 2014; Verney et al., 2011).

The importance of flocculation (instead of resuspension) as the governing process determining particle properties in the investigated system can be observed in the growth of coarse particles at the expense of fine particles (Fig. 5b). In systems where particle properties are governed by resuspension processes, growth of coarse particles takes place without change in the fine particle fractions as previously shown by Brand et al. (2010). We specifically observe small floc sizes at high current velocities (high shear rate G), which was previously attributed to shear instigated floc break up (Figs. 4 and 5 blue and red line; Fig. 6a) (Lee et al., 2012; Winterwerp, 2002). This was followed by floc aggregation as soon as turbulence (G values) decreases, leading to increased floc sizes. The aggregation dominant phase reaches its maximum at high water slack, where maximum floc sizes can be observed. However, the previously observed phenomenon of rapidly settling macro flocs as reported by Verney et al. (2011) and Winterwerp (2002) was not visible during our measurements. The absence of rapid macro floc settling might be explained due to our low position within the water column (20 cmab) and could be indicated through the observed higher temporal variation in floc sizes at high water slack (Figs. 4 and 5a green plane/line, Fig. 6a). The above described mechanism of shear dominated flocculation processes further suggests that at moderate shear a wide range of floc sizes should be present, which is also confirmed by our observations (Figs. 4 and 6a).

The observed negative correlation between shear rate G and mean floc size, i.e. increasing mean floc size values during decreasing shear rate periods (Fig. 6a), is in close agreement with the laboratory experiments conducted by Verney et al. (2011). This suggests that during a large part of the tidal cycle, flocs are in

equilibrium with turbulent shear rates, which controls the balance between floc aggregation and destruction. However the negative correlation seems only present as soon as water depths are above 1.15 m for flood tide and above 0.8 m for ebb tide (Fig. 6a and b). We hypothesize that this is caused by (1) SPM concentrations that are too low to promote floc aggregation at the end of the ebb phase when water levels become very low (Fig. 6b); and (2) due to the import of flocs which are not in equilibrium with the local hydrodynamics at the beginning of the flood phase. We assume that these flocs originate from re-flocculation of flocs from the highly turbulent constriction at the bridge of the Sieperda creek where also rock armor (riprap) is present (Fig. 1).

It is further evident that the dependency of floc size on shear is mainly present during flood (Fig. 6a), whereas during ebb floc size seems to be stronger influenced by SPM concentrations (Fig. 6b). The observed floc dynamics governed by shear rate during flood and their deduced settling velocities are in agreement with previously studies showing turbulence controlled flocculation dynamics (Eisma and Li, 1993; Wang et al., 2013), whereas during ebb our case study seems to resemble a flocculation system controlled by SPM concentration as shown by Dyer and Manning (1999).

Temporal floc size dynamics reveal a counter-clockwise hysteresis for ebb tide, however a less pronounced hysteresis during flood, as previously found by Verney et al. (2011) (Fig. 6a). The proposed mechanism, being differences between aggregation and destruction time scales (herewith time is defined as floc populations reaching a new equilibrium), is still proposed to be one of the governing factors. Where previous studies have shown that flow deceleration promotes direct reduction in floc size, whereas flow acceleration does not instantaneously increase floc aggregation, since it depends on collision rates between particles and their collision efficiency (Verney et al., 2011; Winterwerp, 2002). We propose that the observed difference in flocculation between ebb and flood is more pronounced due to tidal asymmetry, i.e. flood dominance resulting in an asymmetric shear rate which superimposes the previously observed time lag as previously shown by Manning and Schoellhamer (2013) (Figs. 3 and 6c). To our knowledge the only other study observing flocculation hysteresis in the field showed a clockwise hysteresis caused by the formation of large flocs during low shear rates which are destroyed through increased shear rates during accelerating currents (Markussen and Andersen, 2014). However their observed timescales in floc formation and breakup, it took roughly twice the time for floc break-up compared to flocculation, are directly opposed to our results. We observe that it takes roughly twice the time for flocculation processes to occur compared floc break-up processes (Fig. 7b). These differences in timescales between processes of floc aggregation and destruction have important ramifications on settling fluxes. Since not only abiotic factors but also biotic ones are important determinants for floc dynamics, further measurements need to be conducted to elucidate the seasonally controlled influence of biota on flocculation dynamics and consequently settling velocities (Fettweis and Baeye, 2015).

4.2.3. Technical limitations for floc measurements

The LISST is based on light transmittance through a volume of water. Light that is scattered by particles in the water column is received by an array of photodetectors consisting of 32 different log-spaced bins representing 32 different diffraction angles that in turn correspond to different particle size ranges (2.5–500 μm) (Agrawal and Pottsmith, 2000; Voulgaris and Meyers, 2004). Previous studies indicated uncertainties in LISST derived particle size distributions, when open tails at either end of the spectrum are present (Davies et al., 2012; Fettweis and Baeye, 2015; Mikkelsen and Pejrup, 2001). Macrofloc sizes recorded by a video system at an estuarine site with similar tidal dynamics were generally smaller than 580 μm (Winterwerp, 2006), which indicates that most of the large flocs probably exceeded the size limit of the LISST. This maximum floc size limit was also reported by Fettweis and Baeye (2015). Additional uncertainties linked to the measurement of volume concentrations of particles with an equivalent spherical instead of a "true" random shape by the LISST can be assumed to be minimal, since this error is specifically important for rising tails at the low end (<10 μm) of the particle size spectrum which was not observed throughout our measurements (Agrawal et al., 2008). Since no other particle size measures were available, we have to treat the LISST derived floc size as estimates rather than absolute values, however previous comparisons between LISST and floc camera derived floc measurements support the robustness of the observed floc tidal variation (Hill et al., 2013). We can further deduce that maximum floc size potentially increases from measured size estimates of 350 μm, equal to the median of the highest size class of the LISST (Fig. 5b). This will also have ramifications on the calculated settling velocity estimated, suggesting that the calculated settling velocities by the LISST are an underestimation. Despite the uncertainties and limitations of the LISST-100C detectors, which are related to the characteristics of the particles occurring in nature (Andrews et al., 2010; Mikkelsen and Pejrup, 2001) and to the measuring principle itself (Goossens, 2008), it is well suited to collect time series in Particle Size Distributions (PSDs) autonomously.

5. Conclusions

This study confirms that flocculation processes play an important role determining *in-situ* settling velocities in the field. Flocs rather than primary particles determine SPM dynamics and potentially exert an important control on residual transport and sedimentation/erosion processes. The adapted Stoke's Law provided reliable settling velocity estimates regarding to spatio-temporal changes over the tidal cycle, although its estimates were susceptible to changes in suspended particle populations.

An investigation of the limiting assumption of the Reynolds-flux method revealed that vertical fluxes as well as along-channel gradients and its associated horizontal flux divergence limit its applicability in our field situation. The vertical redistribution of suspended particulate matter during acceleration and deceleration of the currents results in a temporal pattern in vertical fluxes redistributing suspended matter over the water column. This temporal pattern is unrelated to an equivalent temporal pattern in gravitational settling, thus limiting the application of the Reynolds-flux method. We additionally show the importance of horizontal flux divergence as another limiting factor in applying the Reynolds-flux method, which together with the vertical redistribution of SPM precludes the application of the Reynolds flux method at our field site.

The fact that the LISST measured the entire particle population (settling and non-settling) at a specific depth (20cmab) whereas the Reynolds-flux method only measures the settling population could not adequately explain the difference found in spatio-temporal settling velocity estimates. This would suggest that under circumstances where both methods are applicable the Reynolds-flux method is expected to produce higher settling velocity estimates than the LISST method. This was not the case since the Reynolds-flux method show only higher estimates during peak velocities, where it's limiting assumption where clearly not fulfilled. We propose that the previously suggest rule of thumb coined by Cartwright et al. (2013) that the Reynolds-Flux method should not be used for near-bed velocities less than 0.2 m s^{-1} (potential importance of the local rate of change term during acceleration and

deceleration) should be extended. Since the presence of along-channel gradients further limits applicability of the Reynolds-Flux method. As shown above a first assessment of along-channel gradients could be done by using scaling arguments or if possible additional field measurements at various depths and along channel locations.

Acknowledgements

We want to thank “Het Zeeuwse Landschap” for facilitating our research in this nature conservatory. We also want to thank the NIOZ-Yerseke for the provided instruments (ADVs), and the VLIZ (“Vlaams Instituut voor de Zee) for facilitating the use of the LISST-100C. Olja Bezdenjesnji and Heather Mariash are thanked for the provided field assistance. This research was financed as part of the Hedwige-Prosper polder project financed by the VNSC, W&Z and the Provincie Zeeland. This research was supported by the Netherlands Organisation for Scientific Research (NWO-VIDI grant no. 864.13.007 to DvO).

References

Agrawal, Y.C., Pottsmith, H.C., 2000. Instruments for particle size and settling velocity observations in sediment transport. Mar. Geol. 168, 89–114. http://dx.doi.org/10.1016/S0025-3227(00)00044-X.

Agrawal, Y.C., Whitmire, A., Mikkelsen, O.A., Pottsmith, H.C., 2008. Light scattering by random shaped particles and consequences on measuring suspended sediments by laser diffraction. J. Geophys. Res. Ocean. 113, C04023. http://dx.doi.org/10.1029/2007JC004403.

Andrews, S., Nover, D., Schladow, S.G., 2010. Using laser diffraction data to obtain accurate particle size distributions: the role of particle composition. Limnol. Oceanogr. Methods 8, 507–526. http://dx.doi.org/10.4319/lom.2010.8.507.

Avoine, J., Allen, G.P., Nichols, M., Salomon, J.C., Larsonneur, C., 1981. Suspended-sediment transport in the Seine estuary, France: effect of man-made modifications on estuary—shelf sedimentology. Mar. Geol. 40, 119–137. http://dx.doi.org/10.1016/0025-3227(81)90046-3.

Brand, A., Lacy, J.R., Hsu, K., Hoover, D., Gladding, S., Stacey, M.T., 2010. Wind-enhanced resuspension in the shallow waters of South San Francisco Bay: mechanisms and potential implications for cohesive sediment transport. J. Geophys. Res. C Ocean. 115, C11024. http://dx.doi.org/10.1029/2010JC006172.

Burchard, H., Flöser, G., Staneva, J.V., Badewien, T.H., Riethmüller, R., 2008. Impact of density gradients on net sediment transport into the Wadden sea. J. Phys. Oceanogr. 38, 566–587. http://dx.doi.org/10.1175/2007JPO3796.1.

Cartwright, G.M., Friedrichs, C.T., Smith, S.J., 2013. A test of the ADV-based Reynolds flux method for in situ estimation of sediment settling velocity in a muddy estuary. Geo-Marine Lett. 33, 477–484. http://dx.doi.org/10.1007/s00367-013-0340-4.

Chen, M.S., Wartel, S., Temmerman, S., 2005. Seasonal variation of floc characteristics on tidal flats, the Scheldt estuary. Hydrobiologia 540, 181–195. http://dx.doi.org/10.1007/s10750-004-7143-6.

Christiansen, T., Wiberg, P., Milligan, T., 2000. Flow and sediment transport on a tidal salt marsh surface. Estuar. Coast. Shelf Sci. 50, 315–331. http://dx.doi.org/10.1006/ecss.2000.0548.

Davies, E.J., Nimmo-Smith, W.A.M., Agrawal, Y.C., Souza, A.J., 2012. LISST-100 response to large particles. Mar. Geol. 307–310, 117–122. http://dx.doi.org/10.1016/j.margeo.2012.03.006.

de Lucas Pardo, M.A., Sarpe, D., Winterwerp, J.C., 2015. Effect of algae on flocculation of suspended bed sediments in a large shallow lake. Consequences for ecology and sediment transport processes. Ocean. Dyn. 65, 889–903. http://dx.doi.org/10.1007/s10236-015-0841-y.

De Vriend, H.J., Wang, Z.B., Ysebaert, T., Herman, P.M.J., Ding, P., 2011. Eco-morphological problems in the yangtze estuary and the Western Scheldt. Wetlands 31, 1033–1042. http://dx.doi.org/10.1007/s13157-011-0239-7.

Dyer, K.R., 1995. Chapter 14 sediment transport processes in estuaries. Dev. Sedimentol. 53, 423–449. http://dx.doi.org/10.1016/S0070-4571(05)80034-2.

Dyer, K.R., 1989. Sediment processes in estuaries: future research requirements. J. Geophys. Res. 94, 14327. http://dx.doi.org/10.1029/JC094iC10p14327.

Dyer, K.R., Manning, A.J., 1999. Observation of the size, settling velocity and effective density of flocs, and their fractal dimensions. J. Sea Res. 87–95. http://dx.doi.org/10.1016/S1385-1101(98)00036-7.

Einstein, H.A., Krone, R.B., 1962. Experiments to determine modes of cohesive sediment transport in salt water. J. Geophys. Res. 67, 1451–1461. http://dx.doi.org/10.1029/JZ067i004p01451.

Eisma, D., 1986. Flocculation and de-flocculation of suspended matter in estuaries. Neth. J. Sea Res. 20, 183–199. http://dx.doi.org/10.1016/0077-7579(86)90041-4.

Eisma, D., Bernard, P., Cadée, G.C., Ittekkot, V., Kalf, J., Laane, R., Martin, J.M., Mook, W.G., van Put, A., Schuhmacher, T., 1991. Suspended-matter particle size in some West-European estuaries; part II: a review on floc formation and break-up. Neth. J. Sea Res. 28, 215–220. http://dx.doi.org/10.1016/0077-7579(91)90018-V.

Eisma, D., Boer, P.L., de Cadee, G.C., Dijkema, K., Ridderinkhof, H., Philippart, C., 1997. Intertidal Deposits: River Mounths, Tidal Flats, and Coastal Lagoons. CRC Press.

Eisma, D., Li, A., 1993. Changes in suspended-matter floc size during the tidal cycle in the dollard estuary. Neth. J. Sea Res. 31, 107–117. http://dx.doi.org/10.1016/0077-7579(93)90001-9.

Fennessy, M.J., Dyer, K.R., Huntley, D.A., 1994. Inssev: an instrument to measure the size and settling velocity of flocs in situ. Mar. Geol. 117, 107–117. http://dx.doi.org/10.1016/0025-3227(94)90009-4.

Fettweis, M., Baeye, M., 2015. Seasonal variation in concentration, size, and settling velocity of muddy marine flocs in the benthic boundary layer. J. Geophys. Res. Ocean. 120, 5648–5667. http://dx.doi.org/10.1002/2014JC010644.

Friedrichs, C., Armbrust, B., Swart, H.D.E., 1998. Hydrodynamics and equilibrium sediment dynamics of shallow, funnel-shaped tidal estuaries. Phys. Estuaries Coast. Seas. 315–327.

Fugate, D.C., Friedrichs, C.T., 2002. Determining concentration and fall velocity of estuarine particle populations using adv, obs and lisst. Cont. Shelf Res. 1867–1886. http://dx.doi.org/10.1016/S0278-4343(02)00043-2.

Galappatti, R., 1983. A Depth Integrated Model for Suspended Transport, Communications on Hydraulics. Department of Civil Engineering, Delft University of Technology.

Goossens, D., 2008. Techniques to measure grain-size distributions of loamy sediments: a comparative study of ten instruments for wet analysis. Sedimentology 55, 65–96. http://dx.doi.org/10.1111/j.1365-3091.2007.00893.x.

Graham, G.W., Manning, A.J., 2007. Floc size and settling velocity within a Spartina anglica canopy. Cont. Shelf Res. 27, 1060–1079. http://dx.doi.org/10.1016/j.csr.2005.11.017.

Hibma, A., Stive, M.J.F., Wang, Z.B., 2004. Estuarine morphodynamics. Coast. Eng. 51, 765–778. http://dx.doi.org/10.1016/j.coastaleng.2004.07.008.

Hill, P.S., Newgard, J.P., Law, B.A., Milligan, T.G., 2013. Flocculation on a muddy intertidal flat in Willapa Bay, Washington, Part II: observations of suspended particle size in a secondary channel and adjacent flat. Cont. Shelf Res. 60, S145–S156. http://dx.doi.org/10.1016/j.csr.2012.06.006.

Hill, P.S., Nowell, A.R.M., Jumars, P.A., 1992. Encounter rate by turbulent shear of particles similar in diameter to the Kolmogorov scale. J. Mar. Res. 50, 643–668. http://dx.doi.org/10.1357/002224092784797539.

Hill, P.S., Syvitski, J.P., Cowan, E.A., Powell, R.D., 1998. In situ observations of floc settling velocities in Glacier Bay, Alaska. Mar. Geol. 145, 85–94. http://dx.doi.org/10.1016/S0025-3227(97)00109-6.

Holtappels, M., Glud, R.N., Donis, D., Liu, B., Hume, A., Wenzhöfer, F., Kuypers, M.M.M., 2013. Effects of transient bottom water currents and oxygen concentrations on benthic exchange rates as assessed by eddy correlation measurements. J. Geophys. Res. Ocean. 118, 1157–1169. http://dx.doi.org/10.1002/jgrc.20112.

Lanzoni, S., Seminara, G., 2002. Long-term evolution and morphodynamic equilibrium of tidal channels. J. Geophys. Res. 107, 3001. http://dx.doi.org/10.1029/2000JC000468.

Lee, B.J., Fettweis, M., Toorman, E., Molz, F.J., 2012. Multimodality of a particle size distribution of cohesive suspended particulate matters in a coastal zone. J. Geophys. Res. Ocean. 117 http://dx.doi.org/10.1029/2011JC007552 n/a-n/a.

Lorke, A., McGinnis, D.F., Maeck, A., 2013. Eddy-correlation measurements of benthic fluxes under complex flow conditions: effects of coordinate transformations and averaging time scales. Limnol. Oceanogr. Methods 11, 425–437. http://dx.doi.org/10.4319/lom.2013.11.425.

Lynch, J.F., Agrawal, Y.C., 1991. A model-dependent method for inverting vertical profiles of scattering to obtain particle size spectra in boundary layers. Mar. Geol. 99, 387–401. http://dx.doi.org/10.1016/0025-3227(91)90051-5.

Lynch, J.F., Irish, J.D., Sherwood, C.R., Agrawal, Y.C., 1994. Determining suspended sediment particle size information from acoustical and optical backscatter measurements. Cont. Shelf Res. 14, 1139–1165. http://dx.doi.org/10.1016/0278-4343(94)90032-9.

Manning, A.J., Langston, W.J., Jonas, P.J.C., 2010. A review of sediment dynamics in the Severn Estuary: influence of flocculation. Mar. Pollut. Bull. 61, 37–51. http://dx.doi.org/10.1016/j.marpolbul.2009.12.012.

Manning, A.J., Schoellhamer, D.H., 2013. Factors controlling floc settling velocity along a longitudinal estuarine transect. Mar. Geol. 345, 266–280. http://dx.doi.org/10.1016/j.margeo.2013.06.018.

Markussen, T.N., Andersen, T.J., 2014. Flocculation and floc break-up related to tidally induced turbulent shear in a low-turbidity, microtidal estuary. J. Sea Res. 89, 1–11. http://dx.doi.org/10.1016/j.seares.2014.02.001.

Markussen, T.N., Andersen, T.J., 2013. A simple method for calculating in situ floc settling velocities based on effective density functions. Mar. Geol. 344, 10–18. http://dx.doi.org/10.1016/j.margeo.2013.07.002.

Mietta, F., Chassagne, C., Manning, A.J., Winterwerp, J.C., 2009. Influence of shear rate, organic matter content, pH and salinity on mud flocculation. Ocean. Dyn. 59, 751–763. http://dx.doi.org/10.1007/s10236-009-0231-4.

Mikkelsen, O.A., Pejrup, M., 2001. The use of a LISST-100 laser particle sizer for in-situ estimates of floc size, density and settling velocity. Geo-Marine Lett. 20, 187–195. http://dx.doi.org/10.1007/s003670100064.

Nardin, W., Edmonds, D.A., 2014. Optimum vegetation height and density for inorganic sedimentation in deltaic marshes. Nat. Geosci. 7, 722–726.

R_Core_Team, 2013. R: A language and environment for statistical computing.

Safak, I., Allison, M.A., Sheremet, A., 2013. Floc variability under changing turbulent stresses and sediment availability on a wave energetic muddy shelf. Cont. Shelf

Res. 53, 1–10. http://dx.doi.org/10.1016/j.csr.2012.11.015.
Salehi, M., Strom, K.B., 2010. Relationship between acoustic backscatter strength and suspended sediment concentration using a 6 MHz Nortek vector velocimeter. World Environ. Water Resour. Congr. 1676–1682. http://dx.doi.org/10.1061/41114(371)176, 2010.
Stevenson, J.C., Ward, L.G., Kearney, M.S., 1988. Sediment transport and trapping in marsh systems: implications of tidal flux studies. Mar. Geol. 80, 37–59. http://dx.doi.org/10.1016/0025-3227(88)90071-0.
Talke, S.A., de Swart, H.E., Schuttelaars, H.M., 2009. Feedback between residual circulations and sediment distribution in highly turbid estuaries: an analytical model. Cont. Shelf Res. 29, 119–135. http://dx.doi.org/10.1016/j.csr.2007.09.002.
Toorman, E., 2003. Validation of macroscopic modelling of particle-laden turbulent flows. Proc. 6th Belg. Natl. Congr. Theor. Appl. Mech. 26–27.
Toorman, E., 2002. Modelling of turbulent flow with suspended cohesive sediment. Proc. Mar. Sci. 5, 155–169. http://dx.doi.org/10.1016/S1568-2692(02)80014-6.
Van Leussen, W., 2011. Macroflocs, fine-grained sediment transports, and their longitudinal variations in the Ems Estuary. Ocean. Dyn. 387–401. http://dx.doi.org/10.1007/s10236-011-0384-9.
Van Leussen, W., 1988. Aggregation of particles, settling velocity of mud flocs a review. In: Physical Processes in Estuaries. Springer, Berlin Heidelberg, pp. 347–403. http://dx.doi.org/10.1007/978-3-642-73691-9_19. Berlin, Heidelberg.
Van Rijn, L.C., 2010. Tidal phenomena in the Scheldt estuary, pp. 1–99. Report, Deltares.
Van Rijn, L.C., 1993. Principles of sediment transport in rivers, estuaries and coastal seas. Princ. Sediment. Transp. Rivers, Estuaries Coast. Seas. 1006.
Verney, R., Lafite, R., Brun-Cottan, J.C., Le Hir, P., 2011. Behaviour of a floc population during a tidal cycle: laboratory experiments and numerical modelling. Cont. Shelf Res. 31 http://dx.doi.org/10.1016/j.csr.2010.02.005.
Vickers, D., Mahrt, L., 1997. Quality control and flux sampling problems for tower and aircraft data. J. Atmos. Ocean. Technol. 14, 512–526. http://dx.doi.org/10.1175/1520-0426(1997)014<0512:QCAFSP>2.0.CO;2.
Voulgaris, G., Meyers, S.T., 2004. Temporal variability of hydrodynamics, sediment concentration and sediment settling velocity in a tidal creek. Cont. Shelf Res. 24, 1659–1683. http://dx.doi.org/10.1016/j.csr.2004.05.006.
Voulgaris, G., Trowbridge, J.H., 1998. Evaluation of the Acoustic Doppler Velocimeter (ADV) for turbulence measurements*. J. Atmos. Ocean. Technol. 15, 272–289. http://dx.doi.org/10.1175/1520-0426(1998)015<0272:EOTADV>2.0.CO;2.
Wang, Y.P., Voulgaris, G., Li, Y., Yang, Y., Gao, J., Chen, J., Gao, S., 2013. Sediment resuspension, flocculation, and settling in a macrotidal estuary. J. Geophys. Res. Ocean. 118, 5591–5608. http://dx.doi.org/10.1002/jgrc.20340.
Wilczak, J.M., Oncley, S.P., Stage, S.A., 2000. Sonic anemometer tilt correction algorithms. Boundary-Layer Meteorol. 99, 24. http://dx.doi.org/10.1023/A.
Winterwerp, J.C., 2006. Stratification effects by fine suspended sediment at low, medium, and very high concentrations. J. Geophys. Res. 111, C05012. http://dx.doi.org/10.1029/2005JC003019.
Winterwerp, J.C., 2002. On the flocculation and settling velocity of esturine mud. Cont. Shelf Res. 22, 1339–1360. http://dx.doi.org/10.1016/S0278-4343(02)00010-9.
Winterwerp, J.C., 1998. A simple model for turbulence induced flocculation of cohesive sediment. J. Hydraul. Res. 36, 309–326. http://dx.doi.org/10.1080/00221689809498621.
Winterwerp, J.C., van Kesteren, W.G.M., 2004. Introduction to the physics of cohesive sediment dynamics in the marine environment. Dev. sedimentology 56.
Woodruff, J.D., Geyer, W.R., Sommerfield, C.K., Driscoll, N.W., 2001. Seasonal variation of sediment deposition in the Hudson River estuary. Mar. Geol. 179, 105–119. http://dx.doi.org/10.1016/S0025-3227(01)00182-7.
Yang, Y., Wang, Y.P., Li, C., Gao, S., Shi, B., Zhou, L., Wang, D., Li, G., Dai, C., 2016. On the variability of near-bed floc size due to complex interactions between turbulence, SSC, settling velocity, effective density and the fractal dimension of flocs. Geo-Marine Lett. 36, 135–149. http://dx.doi.org/10.1007/s00367-016-0434-x.